Reaction Chemistry & Engineering

ROYAL SOCIETY OF CHEMISTRY

PAPER

View Article Online
View Journal

Cite this: DOI: 10.1039/d4re00432a

Unveiling the dynamic CO_2 capture performance of MgO promoted with molten salts and $CaCO_3$ *via* fixed bed reactor experiments†

Theodoros Papalas, *[ab] Andy N. Antzaras[a] and Angeliki A. Lemonidou *[ac]

Received 12th September 2024,
Accepted 22nd October 2024

DOI: 10.1039/d4re00432a

rsc.li/reaction-engineering

Carbonate looping using MgO-based materials has recently ignited scientific interest for CO_2 capture at intermediate temperatures (275–375 °C), with the main limitation being the slow carbonation kinetics of MgO. Molten alkali nitrates and metal carbonates have been identified as promoters that provide an alternative reaction mechanism for an enhanced carbonation rate. However, the evaluation of the ability of these materials to effectively remove CO_2 from a gas feed under realistic reactor configurations is still required. This study investigated the CO_2 capture performance of magnesite-derived MgO promoted with limestone and molten Li, Na and K nitrates under carbonate looping conditions in a fixed bed reactor. The CO_2 capture efficiency was enhanced in the presence of H_2O, by increasing the gas–solid contact time and by decreasing the carbonation temperature. The evaluation demonstrated that ~75% CO_2 stripping of a gas feed with 30% CO_2 concentration at 275 °C and a space velocity of 300 h^{-1} is possible, a performance that highlights and expands the potential and possible applications of MgO-based materials.

1. Introduction

The heavy reliance on fossil fuels to satisfy the global energy requirements has led to a significant increase in CO_2 emissions and severe environmental problems. The mitigation of emissions can be attained by adopting renewable resources, increasing the efficiency of current energy technologies and implementing CO_2 capture, utilisation and storage (CCUS).[1,2] Despite the notable progress in renewable energy technologies, their high costs and low maturity, along with the varying availability across regions and the periodic nature of renewable resources, suggest that the global economy will continue to rely on fossil fuels for the foreseeable future. In contrast, CCUS can be applied by retrofitting fossil fuel-dependent energy systems, such as the heavy industry (cement, steel, and chemicals production), which accounts for 20% of industrial emissions.[3] This approach can help carbon-intensive industries meet the requirements of the energy transition period and operate sustainably in the future. Hence, research should aim to find viable CCUS solutions.

Schemes based on reversible gas–solid reactions between CO_2 and metal oxides, such as carbonate looping, comprise a promising carbon capture technology. CO_2 is captured *via* the carbonation of the metal oxide, while the formed carbonate is transferred and decomposed to a second reactor operating at higher temperatures, enabling the reuse of the metal oxide for carbonation. CaO has been favoured for this technology due to its high CO_2 capture capacity (17.8 mmol CO_2 per g) and fast carbonation kinetics at 550–650 °C.[4–6] Such attributes have enabled the pilot-scale investigation of calcium looping, reaching a technology readiness level of 6–7.[7,8] However, harsh decarbonation temperatures (≥900 °C) are detrimental to the CaO stability and process energy demand, while they make retrofitting of existing industries less flexible, as flue gas is typically available at lower temperatures.[9,10]

MgO has recently gained interest due to the favourable thermodynamics (Fig. 1) for carbonation (eqn (1)) at intermediate temperatures (275–375 °C). With a high theoretical CO_2 capture capacity (24.8 mmol CO_2 per g) and mild decarbonation conditions (400–450 °C), MgO presents a sustainable alternative for flexible CO_2 capture applications.[4,11,12] The main limitation comprises the slow carbonation kinetics, arising from the high lattice energy of MgO and the formation of a non-crystalline carbonate layer of 7 Å thickness in contact with CO_2,[13] resulting in an uptake of less than 0.5 mmol CO_2 per g after 1 h exposure to CO_2.[14,15]

$$MgO_{(s)} + CO_{2(g)} \rightleftarrows MgCO_{3(s)},\ \Delta H^{o}_{298K} = \pm 118\ \text{kJ mol}_{CO_2}^{-1} \quad (1)$$

[a] Department of Chemical Engineering, Aristotle University of Thessaloniki, University Campus, 54124 Thessaloniki, Greece. E-mail: alemonidou@cheng.auth.gr
[b] Department of Chemical Engineering and Biotechnology, University of Cambridge, Philippa Fawcett Drive, CB3 0AS Cambridge, UK. E-mail: tp557@cam.ac.uk
[c] Chemical process & Energy Resource Institute, CPERI/CERTH, 57001 Thermi, Thessaloniki, Greece

† Electronic supplementary information (ESI) available. See DOI: https://doi.org/10.1039/d4re00432a

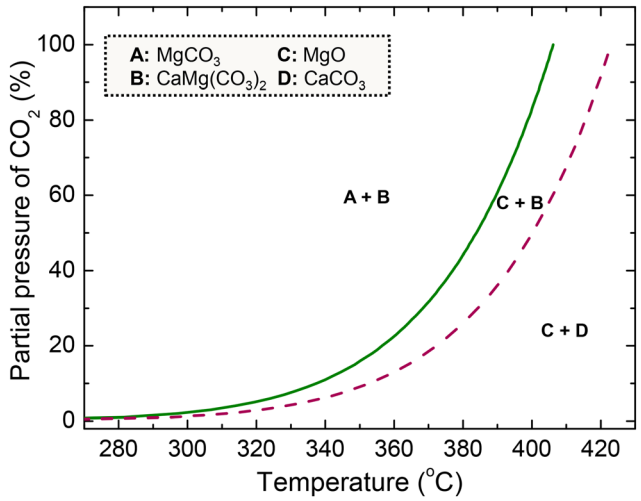

Fig. 1 Equilibrium curves of the carbonation of pure MgO (solid line) and MgO–$CaCO_3$ (dashed line) with a $CaCO_3$ to MgO molar ratio of 0.05 at 1 bar (recreated from ref. 16). In the figure, A refers to $MgCO_3$, B to $CaMg(CO_3)_2$, C to MgO and D to $CaCO_3$.

Zhang *et al.* proposed adding $NaNO_3$ as a promoter in MgO, significantly enhancing the CO_2 capture capacity.[17,18] The ability of $NaNO_3$ to shift to a molten phase under carbonation conditions introduces an alternative reaction mechanism that enables the $MgCO_3$ nuclei formation and growth. They further noted that the molten alkali salt reduces the energy barrier for the dissociation of MgO to $[Mg^{2+}\cdots O^{2-}]$ ionic pairs. The latter reacts with CO_2 adsorbed on the surface of MgO on the triple phase boundaries, or stated otherwise, the contact points between gas, solid and molten phases, to yield $[Mg^{2+}\cdots CO_3^{2-}]$ ionic pairs that eventually crystallise to $MgCO_3$, once the molten phases reach saturation.[18] Dal Pozzo *et al.* also identified the dissolution of MgO to $[Mg^{2+}\cdots O^{2-}]$ ionic pairs as the rate-determining step,[19] while Gao *et al.* found that MgO adsorbs NO_2^+ from the molten phase lowering the barrier of MgO dissolution.[20] Harada *et al.* proposed another carbonation mechanism, suggesting that the molten salt spreads on the surface of MgO and prohibits the formation of non-penetrable carbonate layers. CO_2 dissolved in the molten phase can react with O^{2-} available from $NaNO_3$ to form CO_3^{2-} and then with MgO to generate $MgCO_3$.[21] Other studies supported this mechanism and proved that $MgCO_3$ crystallites have a preferred orientation at the interface between MgO and molten $NaNO_3$, without excluding triple phase boundaries as the formation point of $MgCO_3$.[13,22] Finally, another mechanism proposed by Landuyt *et al.* supports that the MgO surface initially undergoes fast carbonation and the formed carbonates dissolve in $[Mg^{2+}\cdots CO_3^{2-}]$ ionic pairs and then crystallise as $MgCO_3$.[23]

Many researchers have also investigated various binary and ternary salt mixtures except for $NaNO_3$ to evaluate the effect of the composition of the molten phase on the CO_2 capture activity.[19,21,24–26] Addition of alkali nitrates with an alkali of small ionic radius can enhance the CO_2 solubility and thus the CO_2 uptake of the material, while nitrates with an alkali of large ionic radius are resistant to decomposition, thereby retaining their beneficial effect on multiple carbonation and decarbonation cycles.[12,21] Beyond alkali nitrates, there is high interest in using alkali or alkaline earth carbonate promoters (*e.g.* Na_2CO_3, K_2CO_3, $CaCO_3$, $BaCO_3$) to improve the MgO carbonation rate.[27–30] Carbonates serve as nucleation seeds, which are beneficial due to the autocatalytic behaviour of the nuclei formation and growth mechanism. Moreover, they may also form mixed carbonates with MgO, whose formation is thermodynamically feasible at lower partial pressures of CO_2 compared to $MgCO_3$,[13,31,32] as illustrated in Fig. 1 for the case of a mixture of MgO and $CaCO_3$. Our previous work examined MgO-based materials derived from magnesite and promoted with limestone and a mixture of Li, Na and K nitrates (Li/Na/K = 30/18/52). Limestone enabled the formation of $CaMg(CO_3)_2$ and a fast nucleation rate, when applying a $CaCO_3$ to MgO molar ratio of 0.05. Increasing the alkali nitrate content accelerated the generation of carbonates, while the optimal molar ratio of alkali nitrates to MgO was equal to 0.20. The optimum $CaCO_3$ and alkali salt contents resulted in an uptake of 7.2 mmol CO_2 per g (30% CO_2, 300 °C, 30 min) and minimal activity loss (~6%) after 50 cycles in a thermogravimetric analyser.[16,33]

Despite extensive research on molten salt-promoted MgO, the evaluation of CO_2 capture activity has mainly been conducted with pure CO_2 gas feed and long carbonation durations in thermogravimetric analysers, thereby not reflecting realistic operating conditions. Thermogravimetric analysis can efficiently determine the CO_2 uptake capacity of such materials; however, it is essential to also examine the CO_2 stripping efficiency from the gas feed.[12,34] Chen *et al.* evaluated MgO-based materials promoted with various alkali nitrates and carbonates ($LiNO_3$, KNO_3, Na_2CO_3, K_2CO_3) in a fixed bed reactor. They found a CO_2 capture efficiency less than 10% when carbonation was conducted at 325 °C even with the use of a gas feed with unrealistically high CO_2 concentration (80% CO_2) for either pre- or post-combustion CO_2 capture applications.[35] Experiments should be performed under real flow reaction conditions in bench-scale units, with such studies being currently scarce in the literature,[35–40] combined with continuous reactor gas outlet monitoring.

This study builds on our previous work[16,33] and investigates the developed MgO-based material promoted with $CaCO_3$ and alkali nitrates under carbonate looping conditions *via* fixed bed reactor experiments. The ability to remove CO_2 from a gas feed was evaluated by varying temperature, CO_2 concentration, H_2O presence and space velocity. The results of this study reveal the potential and limitations of dynamic CO_2 capture at intermediate temperatures and provide insight on the possible industrial applications of the MgO-based materials.

2. Materials and methods

2.1. Preparation of the material

A MgO-based material was prepared *via* a two-step protocol, initiated by wet mixing of calcined magnesite and calcined limestone in a 12 vol% acetic acid solution and followed by wet impregnation of the resulting solids with Li, Na and K

nitrates (with an atomic ratio of Li/Na/K equal to 30/18/52). The prepared material had nominal molar ratios of $CaCO_3$ and alkali salts to MgO of 0.05 and 0.20, respectively, and was designated as $MgCa_{0.05}A_{0.20}$. The detailed preparation protocol and characterisation results, including *ex situ* and *in situ* X-ray diffraction, N_2 adsorption, and scanning electron microscopy, for both fresh and used materials subjected to carbonate looping conditions can be found elsewhere.[16,33]

2.2. Evaluation of the MgO-based material under carbonate looping conditions

Thermogravimetric analysis (TGA, TG 209 F3 Tarsus, NETZSCH) was utilised to explore the effect of pelletisation on the CO_2 capture activity of the $MgCa_{0.05}A_{0.20}$ material. After the final calcination step of the preparation protocol at 450 °C, the material powders were compressed into small discs with a manual hydraulic press. The discs were then crushed and sieved to obtain a particle size range of 106 to 212 μm. After loading ~10 mg of the material in an Al_2O_3-based crucible, the temperature was increased to 450 °C under a 100% N_2 flow to remove any CO_2 or H_2O captured from the atmosphere. The TGA chamber was cooled down to 300 °C with a rate of 50 °C min^{-1} and the gas feed was switched to a 30% CO_2/N_2 flow for 30 min to conduct the carbonation stage. Afterwards, the sample was heated up to 450 °C at 10 °C min^{-1} to decompose the formed carbonates under a 100% N_2 flow. A total of 50 carbonation and decarbonation cycles were performed, while the same experiment was conducted also with a non-pelletised material for comparison.

The performance of the $MgCa_{0.05}A_{0.20}$ material was investigated by performing experiments in a continuous flow unit equipped with a fixed bed reactor. A schematic illustration of the unit is available in the ESI† (Fig. S1). The reactor was loaded with 0.5, 2, or 4 g of material with a particle diameter below 106 μm obtained by sieving the material without prior pelletisation. Solids were pre-treated by increasing the temperature to 450 °C under a 100% He flow to release any captured CO_2 or H_2O. The reactor was then cooled down to 275, 300 or 325 °C and the gas feed was switched to 30% CO_2/He or 15% CO_2/He (50 mL min^{-1}) to conduct the carbonation stage. The effect of steam was also examined in an experiment, in which the gas feed passed through a steam saturator to attain a 5% H_2O content. The composition of the carbonation gas feed was selected to replicate the flue gas of the cement industry.[41,42] Carbonation was followed by the increase of temperature at 450 °C and the change of gas feed to 100% He (120 mL min^{-1}) to carry out the decarbonation stage. The carbonation and decarbonation stages were repeated for a total of 10 cycles. The duration of the carbonation stage was equal to 30 min, except from the 1st and 10th cycle, where the duration was extended to 60–180 min. The prolonged carbonation stages aimed to fully detect the transition of the kinetically controlled stage to the CO_2 diffusion through the formed carbonate layers, which was different depending on the remaining operating conditions (temperature, CO_2 content in the gas feed, GHSV). On the other hand, decarbonation lasted until the full conversion of carbonates formed in the preceding carbonation stage. In addition to the experiments described, blank experiments were conducted under the same operating conditions with inert SiO_2 that helped to analyse the results. All experiments were conducted at atmospheric pressure, while pressure drop did not display an increase higher than 15% of inlet pressure, satisfying the general rule of thumb for isobaric conditions at laboratory-scale fixed bed reactor experiments. The detailed methodology followed for analysing the results of TGA and reactor experiments is available in the ESI.†

3. Results and discussion

3.1. Evaluation of the effect of pelletisation with thermogravimetric analysis

Prior to the fixed bed experiments, the performance of the $MgCa_{0.05}A_{0.20}$ material was investigated in TGA apparatus to check the effect of pelletisation on the performance of the material to be used in the bench-scale unit. The MgO carbonation conversion and CO_2 capture capacity of the material is presented in Fig. 2. The material sieved to obtain a particle size lower than 106 μm without prior pelletisation displayed an initial CO_2 capture uptake of 7.2 mmol CO_2 per g of material and a high stability, with a minimal 6% activity loss over 50 consecutive carbonation and decarbonation cycles. On the other hand, the material with a particle size between 106 and 212 μm obtained after pelletisation displayed a ~70% lower initial uptake than the non-pelletised material. However, the material exhibited a continuous self-activation, reaching up to 5.4 mmol CO_2 per g of material, while the lower initial activity, coupled with the simultaneous self-activation, agrees with previously reported results in the literature for pelletised MgO.[35,43]

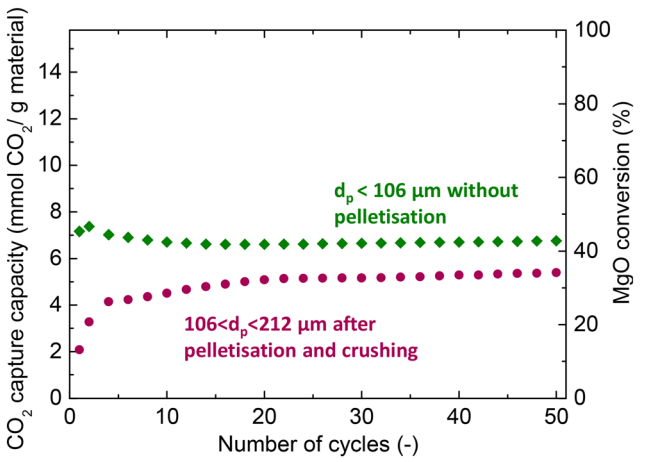

Fig. 2 CO_2 capture efficiency and MgO conversion for the $MgCa_{0.05}A_{0.20}$ material obtained with and without pelletisation when investigated *via* carbonate looping experiments in a thermogravimetric analyser (carbonation stage: 30% CO_2/N_2, 300 °C; decarbonation stage: 450 °C, 100% N_2).

The activity and stability of molten salt-promoted MgO have been linked with various phenomena. While molten salts enhance the CO_2 capture activity, they also dissolve solid components and promote their densification, and thus the annihilation of the pore network, known as liquid phase sintering.[33,44] The cyclic performance is also affected by changes in the distribution of molten salts,[25] as a result of the lower affinity of the molten phase with $MgCO_3$ compared to MgO.[19,32] The re-distribution can be beneficial for the CO_2 capture activity under certain operating conditions and mask the extent of sintering,[33,45] ultimately being the reason behind the stable performance of the non-pelletised material.

Pelletisation caused a decrease of the surface area (from 10.1 to 5.3 $m^2\ g^{-1}$) and pore volume (from 0.08 to 0.03 $cm^3\ g^{-1}$), as found by characterising the materials with N_2 adsorption analysis. The inferior textural properties prevent the efficient distribution and exploitation of molten alkali salts, leading to a lower initial CO_2 uptake.[35] However, Rekhtina *et al.* noted that alkali nitrates can gradually decompose and react with CO_2 to form carbonates, which, as mentioned before, act as nucleation seeds and promote carbonation. They further suggested that this effect accounts for the self-activation phenomenon.[31]

In general, granulation of MgO-based CO_2 capture materials is essential for their practical applications. However, current efforts in this area and existing granulation techniques are limited.[38,40,43] Future research should prioritise the development of MgO granules that exhibit strong mechanical properties and high CO_2 capture ability. A key consideration for any granulation method is its scalability for industrial use, since large quantities of MgO are required for practical looping systems. Additionally, the cost-effectiveness of the manufacturing process is another critical factor.[12] In any case, finding an efficient granulation method was rendered out of the scope of this study and thus all experiments described below were performed using a non-pelletised material with a particle size below 106 μm to evaluate the full potential for stripping CO_2 from a gas feedstock.

3.2. CO_2 capture and release efficiency in a fixed bed reactor

As described before, evaluating the CO_2 capture capacity with TGA does not provide information on the CO_2 capture efficiency from the gas phase, an important parameter for the application of the proposed MgO-based materials. Thus, this section focuses on the performance evaluation under carbonate looping conditions in a fixed bed reactor. Fig. 3a presents the evolution of the CO_2 concentration over time at the exit of the reactor when loaded either with the reactive $MgCa_{0.05}A_{0.20}$ or an inert SiO_2 material (blank experiment). The CO_2 signal was initially zero, reflecting the time needed for the flow to reach the analyser and for the latter to respond. In the blank experiment with SiO_2, the signal gradually increased and stabilised at 30%, the inlet CO_2 concentration. In contrast, the CO_2 signal was noticeably lower in the experiment with $MgCa_{0.05}A_{0.20}$, demonstrating the effective CO_2 capture from the gas phase. It was possible to divide the profile into three regimes, as inferred from other studies.[21,35,40,46] There is an initial period (1st regime) that refers to the time needed for MgO, $CaCO_3$ and CO_2 to be dissolved in the molten salts till saturation and enables the precipitation of the first $MgCO_3$ and $CaMg(CO_3)_2$ nuclei. During this period, CO_2 also reacted with uncoated MgO to form unidentate or bidentate carbonates and this may be the reason behind the extended induction period in the experiment with $MgCa_{0.05}A_{0.20}$ compared to the inert SiO_2 material, as also stated by Zheng *et al.*[40] After some point, the CO_2 capture performance accelerated (2nd regime), since the molten phase remains oversaturated with dissolved reactants, leading to the gradual growth of the size of the nuclei, a faster step compared to their initial formation and the saturation of the molten phase. After some time, the CO_2 diffusion through the formed carbonate layers becomes the kinetically controlled stage, which is slower compared to the previous stages, leading to the gradual reduction of the attained CO_2 capture over time (3rd regime). From an industrial viewpoint, it is preferred to operate before the 3rd regime, where the CO_2 capture is high.

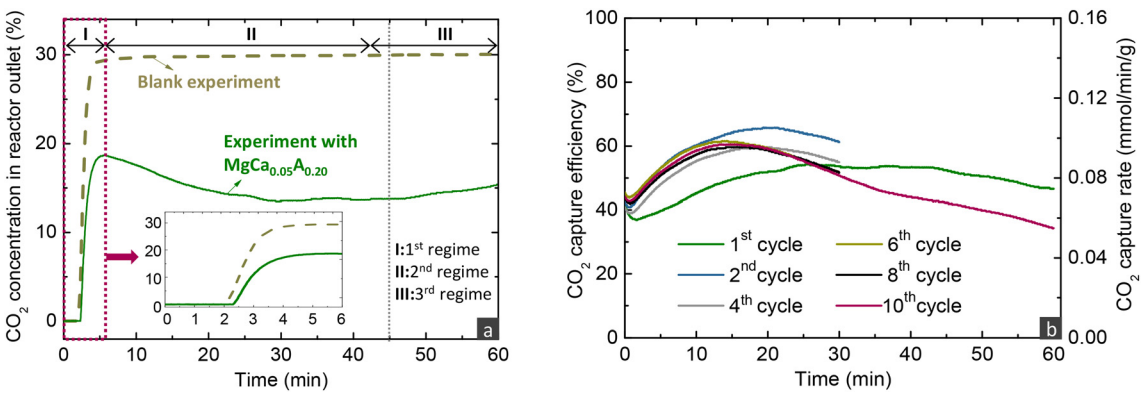

Fig. 3 (a) Outlet CO_2 concentration over time for the blank experiment with SiO_2 and the experiment with the $MgCa_{0.05}A_{0.20}$ material and (b) CO_2 capture efficiency and rate over time for the $MgCa_{0.05}A_{0.20}$ material during the carbonation stage of different cycles when investigated *via* carbonate looping experiments in a fixed bed reactor (carbonation stage: 30% CO_2/He, 300 °C, 300 h^{-1}; decarbonation stage: 450 °C, 100% He, 720 h^{-1}). The inset in figure (a) is the magnification for the first 6 min.

The recorded CO_2 concentration enabled the calculation of the CO_2 capture efficiency and rate, as described in the methodology in the ESI.† Fig. 3b illustrates the results from the investigation of the $MgCa_{0.05}A_{0.20}$ material in 10 consecutive carbonation and decarbonation cycles in a fixed bed reactor containing 4 g of the material. The first and last cycles featured an extended carbonation duration of 60 minutes, while the intermediate cycles lasted 30 minutes each. For simplicity, the data from the first 4 minutes of exposure to CO_2 are excluded from the figure. With the exception of the initial cycle, the CO_2 capture efficiency and rate in the first and second regimes remained consistent throughout the subsequent cycles, attaining a CO_2 capture efficiency and rate of ~60% and ~0.09 mmol min^{-1} g^{-1}, respectively, when exposed to a gas stream with 30% CO_2 concentration at 300 °C. The slightly reduced CO_2 capture performance in the first cycle indicates a lower initial capture capacity; while in subsequent cycles, the material displayed some self-activation, a phenomenon also noted in the literature.[32,33,44]

Fig. 4a displays the outlet CO_2 concentration over time during the decarbonation stage conducted under a 100% He flow, while increasing the temperature to 450 °C. In realistic applications, decarbonation would occur in a CO_2 atmosphere to yield a high-purity CO_2 stream, suitable for sequestration or further use. The performance of the studied material under such conditions was investigated in our previous studies.[16,33] In the current work, the CO_2 release lasted ~9 min for all cycles, with the duration being prolonged only in the 1st and 10th cycle, due to the extended preceding carbonation. In contrast to MgO carbonation, decarbonation was very fast, due to the applied temperature (450 °C), which surpasses the minimum temperatures that thermodynamically allow the full conversion of $MgCO_3$ or $CaMg(CO_3)_2$ compounds (404 and 424 °C as seen in Fig. 1). This implies an enhanced kinetic driving force, which is defined as the difference between the equilibrium CO_2 partial pressure and the actual CO_2 partial pressure ($P_{CO_2,eq} - P_{CO_2}$). Several researchers have mentioned that the molten phase can have a positive effect on the dissociation of carbonate ions and rapid decarbonation of formed carbonates,[21,24,25] while may also initiate at lower temperatures compared to non-promoted MgO.[32,44]

Fig. 4b depicts the MgO and $MgCO_3/CaMg(CO_3)_2$ conversions as determined from the carbonation and decarbonation stages, respectively, following the methodology described in eqn S5 and S6 of the ESI.† Similar carbonation and decarbonation conversions were found, indicating that all the CO_2 captured in each carbonation stage was completely released in the subsequent decarbonation stage. For cycles with a carbonation duration of 30 min, the MgO conversion reached 20%, while the transition to the 3rd regime had taken place before the end of the carbonation stage. The low conversion suggests that applying MgO-based materials in a realistic process would require a reactor with high solids inventory to attain efficient CO_2 capture since after surpassing 20% MgO conversion, the slow CO_2 diffusion controls the reaction rate.

It is important to note that the material displayed high stability over cycles. Even though the solids underwent sintering during cycling operation, as verified by employing X-ray diffraction and by comparing the MgO crystal size between fresh and used materials (Fig. S2 and Table S1 in the ESI†), the high stability is, as mentioned before, a result of a possible alkali salt redistribution in the surface of MgO.[24,33]

3.3. Parametric evaluation for the carbonation stage operation

The effect of the different operating parameters was evaluated by conducting experiments of 10 consecutive carbonation and decarbonation cycles. The figures presented below that illustrate the CO_2 capture efficiency and rate over time profiles contain two curves for each parameter investigated, referring to the first and last carbonation stages of each experiment. Even though the first and last cycles were run for an extended duration (60–180 min) compared to other cycles (30 min), the CO_2 capture

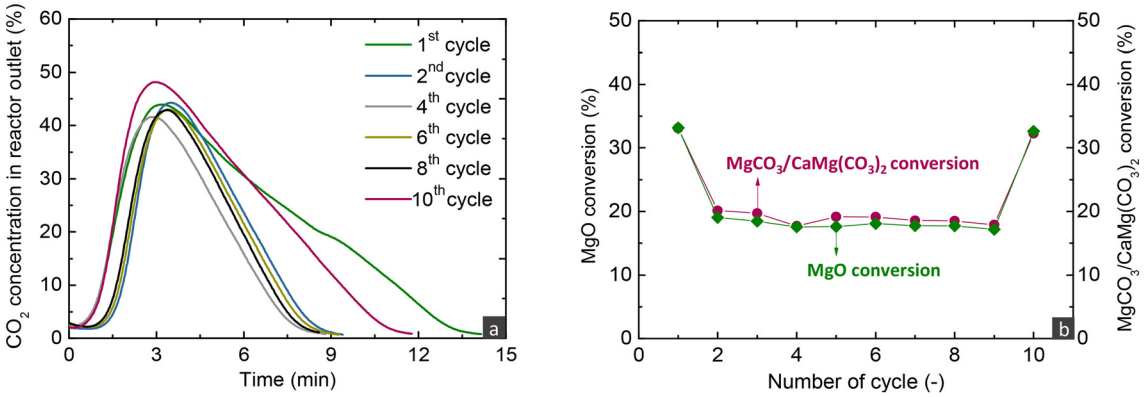

Fig. 4 (a) Outlet CO_2 concentration during the decarbonation stage of different cycles and (b) MgO and $MgCO_3/CaMg(CO_3)_2$ conversions over cycles for the $MgCa_{0.05}A_{0.20}$ material when investigated *via* carbonate looping experiments in a fixed bed reactor (carbonation stage: 30% CO_2/He, 300 °C, 300 h^{-1}; decarbonation stage: 450 °C, 100% He, 720 h^{-1}).

capacity as a function of cycles presented below refer to the CO_2 uptake calculated only from the first 30 min of the carbonation stage.

3.3.1 Effect of space velocity. Fig. 5a presents the activity of the $MgCa_{0.05}A_{0.20}$ material with varying GHSVs, attained by altering the solids inventory. The decrease of GHSV, which increased the gas–solid contact time, affected positively the CO_2 capture efficiency over time, with this effect being more evident when increasing the loading from 0.5 g to 2 g compared to 4 g. The decrease of the CO_2 concentration in the axial direction of the bed leads to a weak kinetic driving force and inefficient trapping of CO_2 in the molten phase at the lower reactor sections and thus a non-proportional CO_2 capture efficiency increase with material loading. This implies that reducing the space velocity to values below 300 h^{-1} would not greatly enhance the CO_2 capture efficiency, as also supported by the declining trend of the CO_2 capture rate (Fig. S3 in the ESI†). Nonetheless, the experiments described below were conducted with a GHSV of 300 h^{-1}, due to the better stripping efficiency. The duration and volumetric gas flow of the experiments with varying GHSV were maintained the same, ultimately leading to higher MgO conversions with a smaller material inventory (Fig. 5b). Despite the different conversion extents, the stability was similar between experiments.

3.3.2 Effect of CO_2 concentration and temperature. Fig. 6 presents the performance of the $MgCa_{0.05}A_{0.20}$ material when investigated at different temperatures (275, 300 and 325 °C) and CO_2 concentrations (30 and 15% CO_2) during the carbonation stage. The stripping efficiency improved with the increase of CO_2 concentration and the decrease of temperature. It is remarkable to note that the CO_2 capture efficiency and rate reached 75% and 0.12 mmol min^{-1} g^{-1}, respectively, when conducting the carbonation at 275 °C with the 30% CO_2/He gas feed in all cycles, except for the first one (Fig. 6a). The better performance when operating the carbonation stage at lower temperature can also be derived from the slightly higher CO_2 capture capacity (Fig. 6b). Reducing the concentration of CO_2 to 15%, a condition which simulates realistic operating conditions for post-combustion CO_2 capture, led to lower CO_2 capture and MgO conversion (Fig. 6c and d), due to the weaker carbonation kinetic driving force. The lower temperature of 275 °C enabled a CO_2 capture of ~60%, while the transition of the kinetically controlled stage to the CO_2 diffusion occurred at lower MgO conversions than the experiment with a 30% CO_2 flow.

Temperature has multiple effects on the carbonation mechanism, as discussed in our previous studies,[16,33] while the current results of fixed bed reactor experiments confirm our initial findings. Increasing the temperature contributes beneficially to the Arrhenius parameter of the reaction rate, but is detrimental to the driving force of carbonation due to the decrease of the $P_{CO_2,eq}$ term. Moreover, temperature affects the solubility of all reactants in the molten phase, with the CO_2 solubility decreasing and the MgO and $CaCO_3$ solubilities increasing at higher temperatures.[21,47] Nonetheless, MgO and $CaCO_3$ exhibit different relationships between their solubility and temperature, with the solubility of MgO promoted at lower temperatures, while the solubility of $CaCO_3$ increases at higher temperatures. Specifically at 275 °C, due to the lower $CaCO_3$ solubility, the $CaMg(CO_3)_2$ phase does not crystallise.[16] Thus, at 275 °C, $CaCO_3$ contributed to the faster kinetics only by acting as a carbonate seed, promoting the formation of the first nuclei. It is worth to mention that following the transition to the 3rd regime, the CO_2 capture efficiency decreased faster over time at lower temperatures, due to the lower diffusivity of CO_2, a phenomenon also seen in CaO-based materials for high-temperature CO_2 capture.[48]

3.3.3 Effect of H_2O addition. All the experiments described above were conducted under dry conditions. However, industrial flue gas contains steam, whose content can reach ~8% in cement production plants or 18–20% in natural gas-fired power plants.[42] The effect of steam addition on the CO_2 capture capacity of molten salt-promoted MgO-based materials has been evaluated *via* TGA experiments,[19,37,49] while in this work, it was examined in the fixed bed reactor (Fig. 7) by

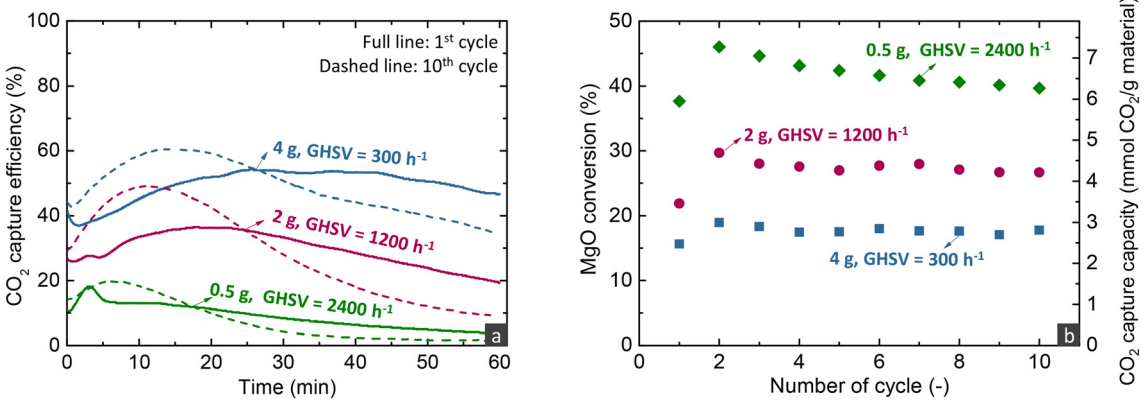

Fig. 5 (a) CO_2 capture efficiency during the carbonation stage of the 1st and 10th cycles and (b) CO_2 capture capacity and MgO conversion over cycles for the $MgCa_{0.05}A_{0.20}$ material when investigated *via* carbonate looping experiments in a fixed bed reactor with different space velocities for the carbonation stage (carbonation stage: 30% CO_2/He, 300 °C; decarbonation stage: 450 °C, 100% He, 720 h^{-1}).

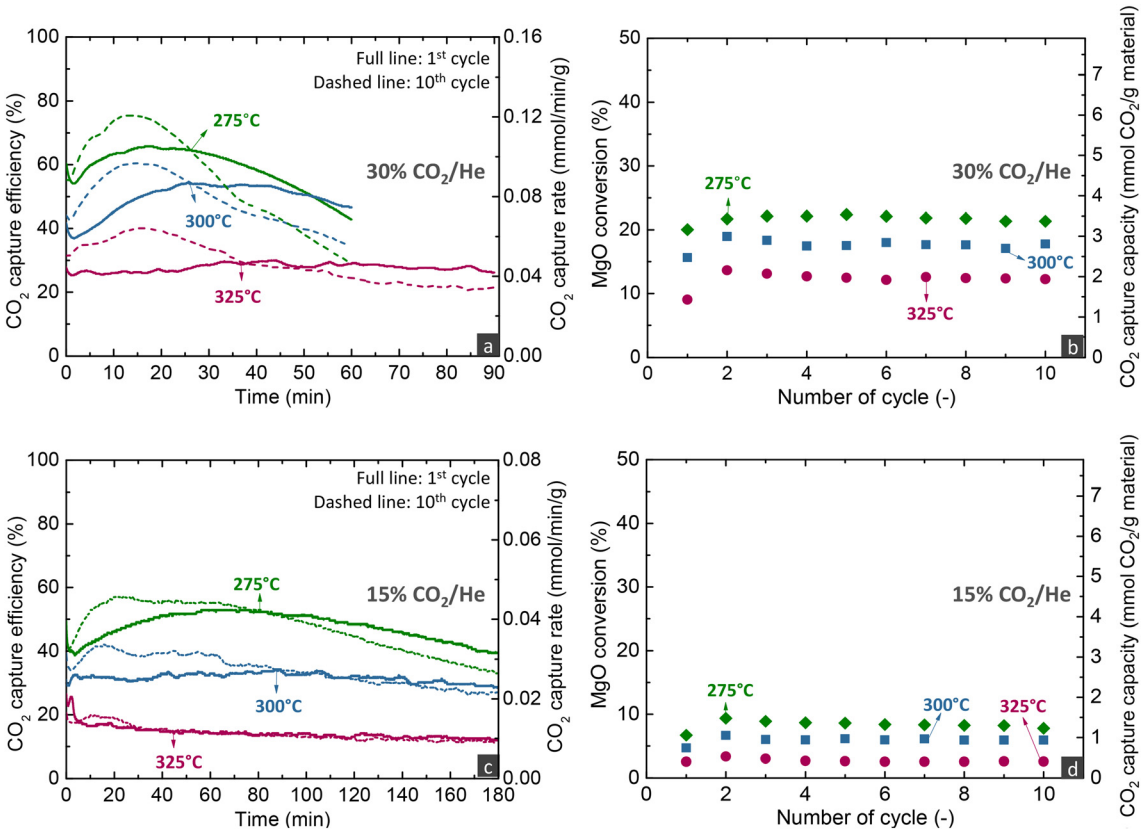

Fig. 6 (a) and (c) CO_2 capture efficiency and rate during the carbonation stage of the 1st and 10th cycles and (b) and (d) CO_2 capture capacity and MgO conversion over cycles for the $MgCa_{0.05}A_{0.20}$ material when investigated *via* carbonate looping experiments in a fixed bed reactor with different temperatures and gas feeds for the carbonation stage (carbonation stage: 300 h^{-1}; decarbonation stage: 450 °C, 100% He, 720 h^{-1}).

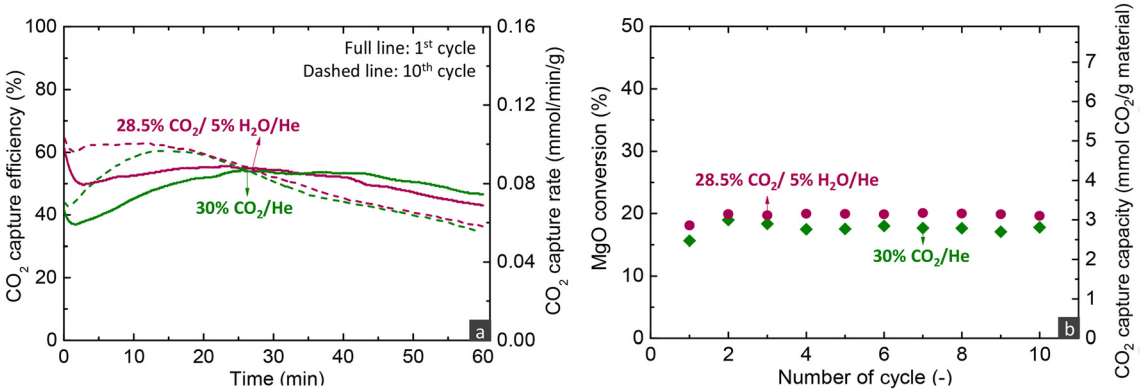

Fig. 7 (a) CO_2 capture efficiency and rate during the carbonation stage of the 1st and 10th cycles and (b) CO_2 capture capacity and MgO conversion over cycles for the $MgCa_{0.05}A_{0.20}$ material when investigated *via* carbonate looping experiments in a fixed bed reactor under dry and wet operating conditions for the carbonation stage (carbonation stage: 300 h^{-1}; decarbonation stage: 450 °C, 100% He, 720 h^{-1}).

applying a gas feed with 5% H_2O content. The latter was attained by passing the dry gas feed of 30% CO_2/He through a steam saturator heated at 33 °C, leading to a wet gas feed composed of 28.5% CO_2/5% H_2O/He. The main difference between the dry and wet operating conditions is the slightly higher and more stable CO_2 capture over time at the beginning of the carbonation stage under the latter conditions, while the CO_2 capture capacity and cyclic stability were not heavily affected. The addition of steam in the gas feed of the carbonation stage of MgO-based materials has been reported to be beneficial for the CO_2 capture efficiency. More specifically, the presence of steam results in the formation of intermediate products, such as MgO with chemisorbed H_2O ($MgO{\cdot}H_2O$) or magnesium hydroxide ($Mg(OH)_2$), which enable the relaxation of the chemical bonds of the MgO lattice, the interaction with CO_2 and initial CO_2 capture. The decomposition of these

components can also reconstruct the pores, which facilitates the diffusion of gas components and promotes the CO_2 capture.[37,50] This work supports that the presence of steam can have a positive effect on the CO_2 capture efficiency and rate.

Overall, the parametric analysis on the carbonation stage revealed that the $MgCa_{0.05}A_{0.20}$ material can attain 75% CO_2 capture efficiency from a gas feed with 30% CO_2 at a significantly low temperature of 275 °C, for low MgO conversions (<20%) in the kinetically controlled regime. However, this result was observed with a quite low space velocity (300 h^{-1}), a performance which contrasts sharply the behaviour of CaO-based materials used for CO_2 capture at high temperatures (600–750 °C). Our previous studies demonstrated that such materials can attain ~90% capture from a gas feed with 12% CO_2 at 650 °C, while the transition of the kinetically controlled stage to the slow CO_2 diffusions occurs after reaching 70% CaO conversion.[5,6] Moreover, the CaO-based materials attained this activity in shorter contact times (GHSV > 5000 h^{-1}) than MgO-based materials (300 h^{-1}).

Even though these discrepancies can be attributed to the different reaction mechanisms of the two materials and the faster carbonation kinetics of CaO mostly because of the higher temperature used, they highlight that CaO-based materials exhibit better CO_2 stripping efficiency compared to MgO-based materials, which indicates that the former materials are perhaps more suitable for post-combustion CO_2 capture applications. However, the promising activity of MgO-based materials and their ability to react with CO_2 at intermediate temperatures merit further investigation, particularly in higher operating pressure applications and the intensification of H_2-producing technologies operating at similar temperatures to MgO, such as sorption-enhanced water gas shift and steam reforming of methanol.[51,52]

4. Conclusions

MgO has emerged as a promising material for CO_2 capture at intermediate temperatures (275–375 °C). However, its broad application has been limited by its slow carbonation kinetics. Recent research has focused on developing MgO-based materials promoted with alkali salts, which enhance the carbonation kinetics *via* an alternative reaction mechanism. Despite extensive evaluations of the CO_2 capture activity of these materials with thermogravimetry, there has been a lack of consideration for the efficiency of stripping CO_2 from a gas feedstock in realistic reactor configurations. In this work, we evaluated a mineral MgO-based material promoted with limestone and Li/Na/K nitrates with molar ratios of $CaCO_3$ and alkali salts to MgO equal to 0.05 and 0.20, respectively, by conducting carbonate looping experiments in a fixed bed reactor. The results showed that carbonation initiates with a high CO_2 capture efficiency and rate, followed by a gradual decrease of performance due to the slow diffusion of CO_2 though the formed carbonate products. The transition between the fast and slow carbonation was found to occur at very low MgO conversions (<20%), dependent on the CO_2 content of the gas feed. The parametric analysis for the carbonation stage revealed that lowering the operating temperature to 275 °C enables ~75% and ~60% CO_2 stripping efficiency from a 30% and 15% CO_2 feed, respectively, while the increase of space velocity and the presence of H_2O promote the carbonation rate. Overall, even though the activity of MgO-based materials for post-combustion CO_2 capture may be inferior to CaO-based materials, the results of this study highlight the potential of MgO-based materials for CO_2 capture and process intensification purposes.

Data availability

The data supporting this article have been included as part of the ESI.†

Author contributions

Theodoros Papalas: conceptualisation, formal analysis, investigation, methodology, validation, visualisation, and writing – original draft. Andy N. Antzaras: validation, supervision, and writing – review & editing. Angeliki A. Lemonidou: supervision, writing – review & editing, resources, project administration, and funding acquisition.

Conflicts of interest

There are no conflicts to declare.

Acknowledgements

This research has been co-financed by the European Regional Development Fund of the European Union and Greek national funds through the Operational Program Competitiveness, Entrepreneurship and Innovation, under the call RESEARCH – CREATE – INNOVATE (project code: T1EDK-01532).

References

1 S. Fawzy, A. I. Osman, J. Doran and D. W. Rooney, *Environ. Chem. Lett.*, 2020, **18**, 2069–2094.
2 IEA, Net zero by 2050: A roadmap for the global energy sector, 2021.
3 IEA, Energy Technology Perspectives 2020 – Special Report on Carbon Capture Utilisation and Storage, 2020.
4 M. T. Dunstan, F. Donat, A. H. Bork, C. P. Grey and C. R. Müller, *Chem. Rev.*, 2021, **121**, 12681–12745.
5 T. Papalas, A. N. Antzaras and A. A. Lemonidou, *Ind. Eng. Chem. Res.*, 2020, **59**, 9926–9938.
6 A. N. Antzara, A. Arregi, E. Heracleous and A. A. Lemonidou, *Chem. Eng. J.*, 2018, **333**, 697–711.
7 J. A. Garcia, M. Villen-Guzman, J. M. Rodriguez-Maroto and J. M. Paz-Garcia, *J. Environ. Chem. Eng.*, 2022, **10**, 108470.
8 S. A. Theofanidis, A. N. Antzaras and A. A. Lemonidou, *Curr. Opin. Chem. Eng.*, 2023, **39**, 1–10.
9 R. Han, Y. Wang, S. Xing, C. Pang, Y. Hao, C. Song and Q. Liu, *Chem. Eng. J.*, 2022, **450**, 137952.

10 J. Chen, L. Duan and Z. Sun, *Energy Fuels*, 2020, **34**, 7806–7836.
11 A. H. Ruhaimi, M. A. A. Aziz and A. A. Jalil, *J. CO2 Util.*, 2020, **43**, 101357.
12 Y. Hu, Y. Guo, J. Sun, H. Li and W. Liu, *J. Mater. Chem. A*, 2019, **7**, 20103–20120.
13 A. H. Bork, M. Rekhtina, E. Willinger, P. Castro-Fernández, J. Drnec, P. M. Abdala and C. R. Müller, *Proc. Natl. Acad. Sci. U. S. A.*, 2021, **118**, e2103971118.
14 K. K. Han, Y. Zhou, W. G. Lin and J. H. Zhu, *Microporous Mesoporous Mater.*, 2013, **169**, 112–119.
15 M. Bhagiyalakshmi, J. Y. Lee and H. T. Jang, *Int. J. Greenhouse Gas Control*, 2010, **4**, 51–56.
16 T. Papalas, I. Polychronidis, A. N. Antzaras and A. A. Lemonidou, *J. CO2 Util.*, 2021, **50**, 101605.
17 K. Zhang, X. S. Li, Y. Duan, D. L. King, P. Singh and L. Li, *Int. J. Greenhouse Gas Control*, 2013, **12**, 351–358.
18 K. Zhang, X. S. Li, W. Z. Li, A. Rohatgi, Y. Duan, P. Singh, L. Li and D. L. King, *Adv. Mater. Interfaces*, 2014, **1**, 1400030.
19 A. Dal Pozzo, A. Armutlulu, M. Rekhtina, P. M. Abdala and C. R. Müller, *ACS Appl. Energy Mater.*, 2019, **2**, 1295–1307.
20 W. Gao, J. Xiao, Q. Wang, S. Li, M. A. Vasiliades, L. Huang, Y. Gao, Q. Jiang, Y. Niu, B. Zhang, Y. Liu, H. He and A. M. Efstathiou, *Adv. Mater.*, 2021, **34**, 2106677.
21 T. Harada, F. Simeon, E. Z. Hamad and T. A. Hatton, *Chem. Mater.*, 2015, **27**, 1943–1949.
22 H. A. Lara-García, W. Gao, A. Gómez-Cortés, G. Diaz, H. Pfeiffer and Q. Wang, *Ind. Eng. Chem. Res.*, 2019, **58**, 5501–5509.
23 A. Landuyt, P. V. Kumar, J. A. Yuwono, A. H. Bork, F. Donat, P. M. Abdala and C. R. Müller, *JACS Au*, 2022, **2**, 2731–2741.
24 H. Jeon, M. L. T. Triviño, S. Hwang, J. H. Moon, J. Yoo and J. G. Seo, *J. CO2 Util.*, 2020, **39**, 101153.
25 H. Lee, M. L. T. Trivinìo, S. Hwang, S. H. Kwon, S. G. Lee, J. H. Moon, J. Yoo and J. G. Seo, *ACS Appl. Mater. Interfaces*, 2018, **10**, 2414–2422.
26 X. Zhao, G. Ji, W. Liu, X. He, E. J. Anthony and M. Zhao, *Chem. Eng. J.*, 2018, **332**, 216–226.
27 A. T. Vu, K. Ho, S. Jin and C. H. Lee, *Chem. Eng. J.*, 2016, **291**, 161–173.
28 H. Cui, Q. Zhang, Y. Hu, C. Peng, X. Fang, Z. Cheng, V. V. Galvita and Z. Zhou, *ACS Appl. Mater. Interfaces*, 2018, **10**, 20611–20620.
29 H. Cui, Z. Cheng and Z. Zhou, *J. Mater. Chem. A*, 2020, **8**, 18280–18291.
30 L. Wang, Z. Zhou, Y. Hu, Z. Cheng and X. Fang, *Ind. Eng. Chem. Res.*, 2017, **56**, 5802–5812.
31 M. Rekhtina, M. Krödel, Y. H. Wu, A. Kierzkowska, F. Donat, P. M. Abdala and C. R. Müller, *Sci. Adv.*, 2023, **9**, eadg5690.
32 S. I. Jo, Y. I. An, K. Y. Kim, S. Y. Choi, J. S. Kwak, K. R. Oh and Y. U. Kwon, *Phys. Chem. Chem. Phys.*, 2017, **17**, 6224–6232.
33 T. Papalas, A. N. Antzaras and A. A. Lemonidou, *J. CO2 Util.*, 2021, **53**, 101725.
34 F. Donat and C. R. Müller, *Curr. Opin. Green Sustainable Chem.*, 2022, **36**, 100645.
35 J. Chen, L. Duan, F. Donat and C. R. Müller, *ACS Sustainable Chem. Eng.*, 2021, **9**, 6659–6672.
36 P. Teixeira, P. Correia and C. I. C. Pinheiro, *Chem. Eng. Sci.*, 2024, **289**, 119856.
37 G. Bang, K.-M. Kim, S. Jin and C.-H. Lee, *Chem. Eng. J.*, 2022, **433**, 134607.
38 Y. Cai, W. Liu, Z. Sun, Y. Yang and P. Li, *J. CO2 Util.*, 2022, **61**, 102047.
39 K. H. Chai, L. K. Leong, S. Sethupathi, K. C. Chong, T. C. K. Yang, S. P. Ong and Y. H. Yap, *Chem. Eng. J. Adv.*, 2024, **17**, 100578.
40 Y. Zheng, J. Wu, L. Zhang, Y. Guo, Z. Xu, Y. Huang, P. Huang, J. Zhang and C. Zhao, *Chem. Eng. J.*, 2022, **450**, 137944.
41 A. Samanta, A. Zhao, G. K. H. Shimizu, P. Sarkar and R. Gupta, *Ind. Eng. Chem. Res.*, 2012, **51**, 1438–1463.
42 D. Ipsakis, G. Varvoutis, A. Lampropoulos, S. Papaefthimiou, G. E. Marnellos and M. Konsolakis, *Renewable Energy*, 2021, **179**, 1884–1896.
43 Y. Hu, X. Liu, Z. Zhou, W. Liu and M. Xu, *Fuel*, 2017, **187**, 328–337.
44 S. Jin, K. Ho, A. T. Vu and C. H. Lee, *Energy Fuels*, 2017, **31**, 9725–9735.
45 X. Ma, H. Cui, Z. Cheng and Z. Zhou, *AIChE J.*, 2023, **69**, e18146.
46 W. Gao, M. A. Vasiliades, C. M. Damaskinos, M. Zhao, W. Fan, Q. Wang, T. R. Reina and A. M. Efstathiou, *Environ. Sci. Technol.*, 2021, **55**, 4513–4521.
47 T. Harada and T. A. Hatton, *Chem. Mater.*, 2015, **27**, 8153–8161.
48 Y. A. Criado, B. Arias and J. C. Abanades, *Ind. Eng. Chem. Res.*, 2018, **57**, 12595–12599.
49 S. Jin, K. Ho and C. H. Lee, *Chem. Eng. J.*, 2018, **333**, 697–711.
50 W. Gao, L. Sun and Q. Wang, in *Pre-combustion Carbon Dioxide Capture Materials*, ed. Q. Wang, Royal Society of Chemistry, 2018, pp. 61–143.
51 Y. Hu, H. Cui, Z. Cheng and Z. Zhou, *Chem. Eng. J.*, 2018, **377**, 119823.
52 H. Li, H. Tian, S. Chen, Z. Sun, T. Liu, R. Liu, S. Assabumrungrat, J. Saupsor, R. Mu, C. Pei and J. Gong, *Appl. Catal., B*, 2020, **276**, 119052.